Available online at www.sciencedirect.com
ScienceDirect
Journal of Power Sources 170 (2007) 242–250
JOURNAL OF POWER SOURCES
www.elsevier.com/locate/jpowsour

Synthesis and characterization of PtRuMo/C nanoparticle electrocatalyst for direct ethanol fuel cell

Zhen-Bo Wang [a,*], Ge-Ping Yin [a], Yong-Ge Lin [b]

[a] *Department of Applied Chemistry, Harbin Institute of Technology, Harbin 150001, China*
[b] *Department of Chemistry, University of Puerto Rico, Rio Piedras Campus, San Juan, PR 00931,USA*

Received 13 February 2007; received in revised form 26 March 2007; accepted 29 March 2007
Available online 20 April 2007

Abstract

This research aims at enhancement of the performance of anodic catalysts for the direct ethanol fuel cell (DEFC). Two distinct DEFC nanoparticle electrocatalysts, PtRuMo/C and PtRu/C, were prepared and characterized, and one glassy carbon working electrode for each was employed to evaluate the catalytic performance. The cyclic-voltammetric, chronoamperometric, and amperometric current–time measurements were done in the solution 0.5 mol L^{-1} CH_3CH_2OH and 0.5 mol L^{-1} H_2SO_4. The composition, particle sizes, lattice parameters, morphology, and the oxidation states of the metals on nanoparticle catalyst surfaces were determined by energy dispersive analysis of X-ray (EDAX), X-ray diffraction (XRD), transmission electron micrographs (TEM) and X-ray photoelectron spectrometer (XPS), respectively. The results of XRD analysis showed that both PtRuMo/C and PtRu/C had a face-centered cubic (fcc) structure with smaller lattice parameters than that of pure platinum. The typical particle sizes were only about 2.5 nm. Both electrodes showed essentially the same onset potential as shown in the CV for ethanol electrooxidation. Despite their comparable active specific areas, PtRuMo/C was superior to PtRu/C in respect of the catalytic activity, durability and CO-tolerance. The effect of Mo in the PtRuMo/C nanoparticle catalyst was illustrated with a bifunctional mechanism, hydrogen-spillover effect and the modification on the Pt electronic states.

Keywords: Direct ethanol fuel cell; PtRuMo/C nanoparticle electrocatalyst; PtRu/C nanoparticle electrocatalyst; Ethanol electrooxidation

1. Introduction

In the past decades, the direct methanol fuel cell (DMFC) has drawn attention for its simple construction with reduced dimensions and high-energy efficiency. Progress has been made in this field [1–3]. However, the intrinsic DMFC disadvantage is the toxicity of methanol. Therefore, researchers have looked for other small molecule alcohols as alternative fuels [4,5]. Ethanol has emerged as the first choice because it is a non-toxicity and low volatility together with a higher energy density than methanol (8.01 kWh kg^{-1} versus 6.09 kWh kg^{-1}) [6]. Other important considerations for choosing ethanol are its low price and its transportability. Among the published reports on proton exchange membrane fuel cells (PEMFC) with alcohol as fuel [5–9], the direct ethanol fuel cell (DEFC) seems promising, especially for the application in devices like electric vehicles, mobile telephone and laptops. However, the complete oxidation of ethanol in DEFC remains the crux of the matter, because, unlike the case of DMFC, it is necessary to break the C–C bond of ethanol at low temperatures. The key is to find an effective anode nanoparticle catalyst. A lot of efforts have been reported [10,11], but all involved catalysts based on Pt, in spite of its limited capability for breaking the C–C bond and its vulnerability to be poisoned at the surface by strongly adsorbed species like CO, which originates from the dissociation of the organic molecules. Thus the sluggish anodic kinetic process for ethanol electrooxidation cannot be avoided, especially at low temperatures. One possible way is to modify the electrode surface to increase at low potentials its coverage of oxygenated species (e.g. adsorbed OH) generated by the dissociation of water, which are necessary to oxidize completely the intermediate species from the dissociation of ethanol to CO_2. At present, there are only a limited number of possible metals which are able to activate water at a low potential with a sufficient stability in acid medium, includ-

* Corresponding author. Tel.: +86 451 86413721; fax: +86 451 86413707.
E-mail address: wangzhenbo1008@yahoo.com.cn (Z.-B. Wang).

0378-7753/$ – see front matter © 2007 Elsevier B.V. All rights reserved.
doi:10.1016/j.jpowsour.2007.03.078

ing Ru [10,12,13], Mo [14,15], Sn [16,17], Os [18], W [19], Ir [20], and so on. PtRu alloys, which have been widely used as catalysts in DMFCs, are still considered to be the best starting point in DEFC research, but their practical use as catalysts for ethanol electrooxidation requires some significant enhancements to the catalytic activities [21]. On the other hand, due to the limited amount of platinum, it is an imperative to minimize or eliminate the usage of this noble metal in catalysts, in consideration of the possible social consequence of the platinum consumption accompanied by successful PEMFC commercialization in the near future.

The addition of a third metal is one of the obvious choices for improving the performance of the electrode and lowering the usage of noble metals [22–24], but the durability of such electrodes could pose an obstacle. Molybdenum, an inexpensive and amply available metal element, has revealed a remarkable effect for promoting the oxidation of CO [25–27] and methanol [28,29]. Recently, both experimental and theoretical studies have suggested that Pt-Mo could be a better catalyst for CO oxidation than PtRu [26,30,31]. As compared with the extensive studies on the carbon supported PtMo binary anodic catalysts in DMFC [23,25,28,29], few reports have been published on ternary alloy nanoparticles (PtRuMo) as anode catalysts for DMFC [32], much less for DEFC. Now, it is apparently the right time to explore the catalytic properties of PtRuMo/C nanoparticles prepared by chemical reduction. This investigation has been carried out with our synthesized PtRuMo/C nanoparticles, aiming for the better approach to enhance the performance of the DEFC anodic catalysts. The results are compared to those obtained with the PtRu/C nanoparticles, which were similarly prepared by chemical reduction of the same precursors with sodium borohydride. X-Ray diffraction (XRD), transmission electron micrographs (TEM), energy dispersive analysis of X-ray (EDAX), and X-ray photoelectron spectrometer (XPS) were used to characterize the catalysts. The catalytic performances were evaluated by the cyclic-voltammetric, chronoamperometric, and amperometric current–time measurements.

2. Experimental

2.1. Preparation of nanoparticle electrocatalysts

The preparation of the PtRuMo/C and the PtRu/C nanoparticles were done as previously described [7,24,33]. All the prepared samples consisted of 20% metal in weight, with the carbon black powder (Vulcan XC-72, Cabot) served as the support. Sodium borohydride was used to chemically reduce the precursors of $Pt(NH_3)_2(NO_2)_2$, $Ru(NO_3)_2$, and $(NH_4)_6Mo_7O_{24}$ at 80 °C to obtain 0.25 g of PtRu (with an atomic ratio of 1:1) or PtRuMo (with an atomic ratio of 6:3:1) nanoparticles supported on carbon. Carbon black was dispersed in a mixture of ultra-pure water and isopropyl alcohol with 20 min of ultrasonication to make a uniform carbon ink. Then the precursors were added to the ink ultrasonically for 15 min. The pH value of the mixture was adjusted by NaOH solution to 8 and then its temperature was raised to 80 °C, immediately before the drop-by-drop addition of 25 mL of 0.2 mol L^{-1} solution of sodium borohydride, which was followed by stirring the bath for 1 h. The product was cooled, dried and washed repeatedly with ultra-pure water (18.2 MΩ cm) until no Na^+ and $B(OH)_4^-$ ions were detected. The formed powder of catalyst was dried for 3 h at 120 °C and then stored in a vacuum vessel. All chemicals here were of analytical grade.

2.2. Electrode preparation and electrochemical measurement

2.2.1. Preparation of working electrode

Three millimeter diameter glassy carbon working electrodes (electrode area 0.0706 cm^2), polished with 0.05 μm alumina to a mirror-finish before each experiment, were used as substrates for the Vulcan-supported catalysts. For the electrode preparation, 5 μL of an ultrasonically redispersed catalyst suspension was pipetted on to the glassy carbon substrate. After the solvent evaporation, the deposited catalyst (28 $\mu g_{metal}\,cm^{-2}$) was covered with 5 μL of a dilute aqueous Nafion solution. The resulting Nafion film with a thickness of ≤0.2 μm has a sufficient strength to attach the Vulcan particles permanently to the glassy carbon electrode without producing significant film diffusion resistances [34].

2.2.2. Electrochemical measurements

All measurements were carried out in the conventional three-electrode electrochemical cell at 25 °C, in which the glassy carbon electrode made in the above mentioned procedure served as the working electrode and a piece of Pt foil (1 cm^2) as the counter electrode. The reference electrode was a reversible hydrogen electrode (RHE) with its solution connected to the working electrode by a Luggin capillary, the tip of which was placed appropriately close to the working electrode. All potential values are versus RHE. All solutions were prepared with the chemicals of analytical grade and the ultra-pure water (MilliQ, Millipore, 18.2 MΩ cm). The ultra-pure argon gas was utilized to continuously purge the solution system of 0.5 mol L^{-1} CH_3CH_2OH and 0.5 mol L^{-1} H_2SO_4, which was kept under constantly stirring state. The cyclic voltammograms (CV) were plotted within a potential range from 0.05 to 1.2 V at a scanning rate of 0.02 V s^{-1}. The chronoamperometric and amperometic *i–t* experiments were done with CHI630A electrochemical analysis instrument controlled by an IBM PC. The potential jumped from 0.1 to 0.8 V. Due to a slight contamination from the Nafion film, the working electrodes were cycled at 0.05 V s^{-1} until the reproducible CV plots were obtained before the measurement curves were recorded. Each separate measurement was always done in the fresh electrolyte.

2.2.3. CO stripping voltammetry

The electrode was electrochemically cleaned in an Ar-degassed solution of 0.5 mol L^{-1} H_2SO_4 solution at 25 °C. The amount of Pt-Ru/C or PtRuMo/C catalyst as the working electrode was 10 μg (28 $\mu g_{metal}\,cm^{-2}$). CO was adsorbed on the surface of the Pt-Ru/C or PtRuMo/C catalyst at 0.08V by bubbling CO gas through the 0.5 mol L^{-1} H_2SO_4 solution for 25 min. The CO dissolved in the solution was subsequently

removed by bubbling argon gas of high purity for 35 min, keeping the potential also at 0.08 V. The potential was then cycled at a scanning rate of 0.02 V s^{-1} from 0.05 to 1.2 V for two oxidation and reduction cycles.

2.3. Characterization of physical properties

2.3.1. X-ray diffraction (XRD)

XRD analysis was accomplished by a D/max-rB diffractometer (made in Japan) with the Cu Kα X-ray source, which was operating at 45 kV and 100 mA. The XRD patterns were generated by the 2θ scan with the scanning rate of 4° min^{-1} and the angular resolution of 0.05°.

2.3.2. Energy dispersive analysis of X-ray (EDAX)

Chemical composition analysis by EDAX was performed with an EDAX Hitachi-S-4700 analyser associated to a scanning electron microscope (SEM, Hitachi Ltd. S-4700). Incident electron beam energies from 3 to 30 keV had been used. In all cases, the beam was at normal incidence to the sample surface and the measurement time was 100 s. All the EDAX spectra were corrected by using the ZAF correction, which takes into account the influence of the matrix material on the obtained spectra.

2.3.3. Transmission electron microscopy (TEM)

Before taking the electron micrographs, the nanoparticle catalyst samples were finely ground and ultrasonically dispersed in isopropanol, a drop of the resultant dispersion was deposited and then dried on the standard copper grid, which was pre-coated with the polymer film. Transmission electron micrographs were taken through a JEOLJEM-1200EX Microscope (made in Japan), operating at the applied voltage of 100 kV, with a magnification of 200,000 and the spatial resolution of 1 nm.

2.3.4. X-ray photoelectron spectrometry (XPS)

The XPS study of surface composition involved a special X-ray photoelectron spectrometer (VG ESCALAB MKII), with the Al Kα X-ray source of 1486.6 eV, which recorded the spectra from the 45° takeoff-angle at the chamber pressure below 5×10^{-9} Pa. The C 1s electron binding energy was referenced at 284.6 eV, and a nonlinear least-squares curve-fitting program was employed with a Gaussian–Lorentzian production function [35,36]. The deconvolution of the XPS spectra was achieved with the reported procedures [21,35–39].

3. Result and discussion

3.1. XRD characterization

The XRD patterns of PtRuMo/C and PtRu/C nanoparticle catalysts in Fig. 1 reveal the structural information, both for metals in bulk and for their carbon support. The first broad peak located at the 2θ value of about 24.8° can be attributed to the carbon support; whereas the four other peaks, which correspond to the Pt crystal planes of (1 1 1), (2 0 0), (2 2 0), and (3 1 1), respectively, are characteristic of the face-centered cubic (fcc) crystalline Pt (JCPDS-ICDD, Card No. 04-802). These patterns indicate the dominant feature of the disordered single-phase structures (i.e. solid solutions) for the alloy. The diffraction peaks of pure Pt are extracted from the database of the Joint Committee on Powder Diffraction Data (JCPDS-ICDD) and also indicated in Fig. 1 by the four vertical lines. It can be seen that the peaks of PtRuMo/C and PtRu/C are shifted to the slightly higher 2θ values. The lack of characteristic peaks of Ru, Mo, and their oxides/hydroxides suggests the possibility that Ru and Mo atoms either form alloys with Pt atoms or exist as oxides in amorphous phases.

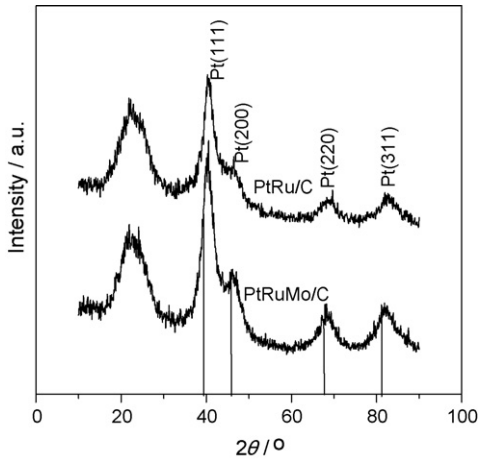

Fig. 1. XRD patterns of the PtRuMo/C and the PtRu/C nanoparticle electrocatalysts.

The data in Table 1, which are based on the Pt (2 2 0) crystal face, not only reflect the formation of a solid solution but also demonstrate the fact that the lattice parameters of both PtRuMo/C and PtRu/C nanoparticles are smaller than those of Pt/C. The progressive decrease in lattice parameters of the alloy corresponds to the progressive increase in the incorporation of Ru and Mo into the alloy state. No significant difference has been found in Table 1 between PtRuMo/C and PtRu/C with respect to the average particle sizes and specific surface areas, which are estimated from full width at half maximum (FWHM) according to Debye–Scherrer formula [40–42] as follows:

$$d = \frac{k\lambda}{\beta_{1/2}\cos\theta} \quad (1)$$

$$S = \frac{60,000}{\rho d} \quad (2)$$

$$\rho_{\text{Pt-Ru}} = X_{\text{Pt}} \times \rho_{\text{Pt}} + X_{\text{Ru}} \times \rho_{\text{Ru}} \quad (3)$$

$$\rho_{\text{Pt-Ru-Ni}} = X_{\text{Pt}} \times \rho_{\text{Pt}} + X_{\text{Ru}} \times \rho_{\text{Ru}} + X_{\text{Mo}} \times \rho_{\text{Mo}} \quad (4)$$

where d is the average particle size (Å), λ the wave length of X-ray (1.5406 Å), θ the angle, at which the peak maximum occurs, $\beta_{1/2}$ the width (in radians) of the diffraction peak at a half height, k a coefficient of 0.89 to 1.39 (0.9 here), ρ the density of Pt-Ru or Pt-Ru-Mo alloy nanoparticles, ρ_{Pt} the density of Pt metal (21.4 g cm^{-3}), ρ_{Ru} the density of Ru metal (12.3 g cm^{-3}), ρ_{Mo} the density of Mo metal (10.3 g cm^{-3}), and X_{Pt}, X_{Ru}, and X_{Mo} are the weight percent of Pt, Ru, and Mo, respectively, in the catalysts.

Table 1
The lattice parameter, particle size, and specific area of the PtRuMo/C and the PtRu/C nanoparticle electrocatalysts

Catalysts	2θ (°)	d-Value (nm)	Lattice parameter (nm)	Particle size (nm)	Specific area ($m^2\ g^{-1}$)
Pt/C	67.70	0.13873	0.3924	–	–
PtRu/C	68.65	0.13634	0.3856	2.7	123.5
PtRuMo/C	68.22	0.13655	0.3862	2.5	126.4

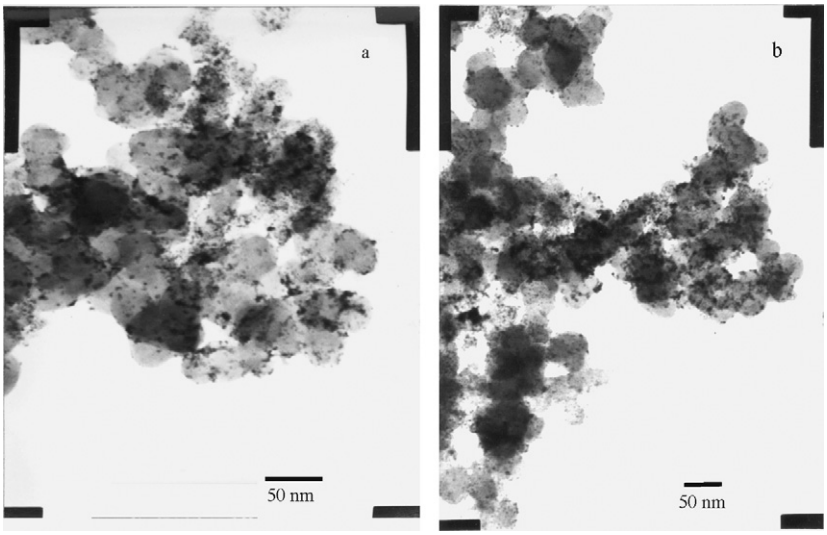

Fig. 2. TEM micrographs of the PtRuMo/C (a) and the PtRu/C (b) nanoparticle electrocatalysts.

3.2. TEM exploration

TEM images obtained from PtRuMo/C and PtRu/C nanoparticles reflect the effect of Mo on the particle size and morphology, which are believed to exert a strong influence on the catalyst properties. The typical bright field TEM micrographs of PtRuMo/C and PtRu/C are presented in Fig. 2a and b, respectively, with metal grains in black and carbon support in grey. It is clearly shown that the spherical metal particles spread homogeneously on carbon grains in both catalyst systems.

In the histograms of the particle sizes (see Fig. 3a for PtRuMo/C and 3b for PtRu/C), the similar peak positions at around 3 nm can be identified. The particle sizes range from 1 to 6 nm for PtRuMo/C and from 1 to 7 nm for PtRu/C, with the average values of 2.8 nm for the former and 2.9 nm for the latter, which are computed from TEM measurement of a series of distinct particle diameters, coded individually with numbers, with the established equation [43] as follows:

$$\bar{d}_n = \frac{\sum_{i=1}^{n} d_i}{n} \tag{5}$$

where $\bar{d}_n$ is the averaged value of all particle diameters in nanometer, n the total number of codes used to identify all the distinct diameters, d_i is the value of the i-coded diameter.

The similarity of particle size distribution is of the implication that the size factor plays no significant role in

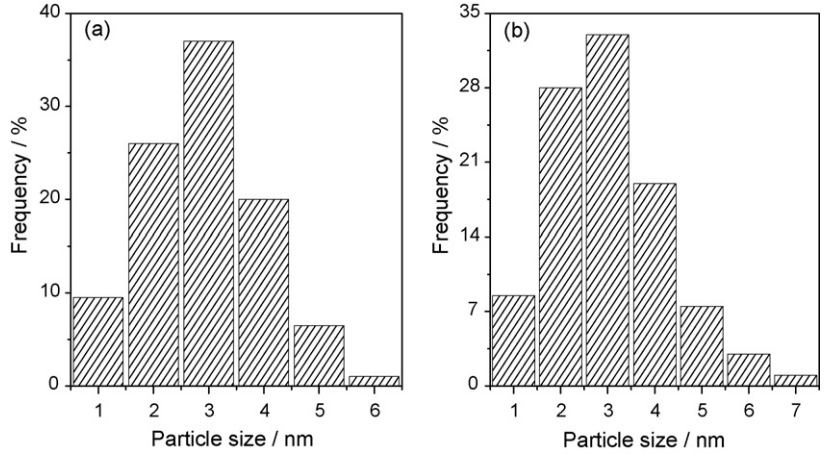

Fig. 3. Size distribution of nanoparticles of the PtRuMo/C (a) and the PtRu/C (b) electrocatalysts.

Table 2
The atomic composition of the PtRuMo/C and the PtRu/C nanoparticles (at.%)

Catalysts	Nominal content			Determined by EDAX		
	Pt	Ru	Mo	Pt	Ru	Mo
PtRu/C	50	50	–	55.9	44.1	–
PtRuMo/C	60	30	10	63.7	26.2	10.1

differentiating the catalytic activity between PtRuMo/C and PtRu/C.

3.3. EDAX analysis

Table 2 shows the actual chemical compositions of PtRuMo/C and PtRu/C nanoparticles catalysts, determined by EDAX detections, which come up with the similar result for different same regions. The atomic ratios among metals are 6.31(Pt):2.59(Ru):1(Mo) for PtRuMo/C and 1.26(Pt):1(Ru) for PtRu/C, close to the formula values.

3.4. Electrochemically active specific area

The electrochemically active specific area (S_{EAS}), which reflects the intrinsic electrocatalytic activity of a catalyst, is calculated with the recognized method based on the curves of CO stripping voltammetry [44,45], through the Eq. (6) as follows:

$$S_{EAS} = \frac{Q_{CO}}{G \times 420} \quad (6)$$

where Q_{CO} is the charge quantity for CO desorption electrooxidation in microcoulomb (μC), and 420 ($\mu C\,cm^{-2}$) the charge required to oxidize a monolayer of CO on alloy catalyst, and G represents the total metal loading (μg) in the electrode.

The calculation results in the similar S_{EAS} values, $106.8\,m^2\,g^{-1}$ for PtRuMo/C and $102.3\,m^2\,g^{-1}$ for PtRu/C. Therefore, S_{EAS} may be excluded from the major factors for the distinction of their catalytic activities.

3.5. Evaluation of catalytic activities

A lot of recent studies focused on the ethanol oxidation with Pt-based catalysts [10,11,18,46–49] have led to a generally accepted mechanism for the ethanol oxidation. In the first step, the cleavage of O–H bond, which is similar to that in the methanol oxidation, generates ethoxy species of CH_3CH_2O, which is subsequently transformed into acetaldehyde CH_3CHO. The final step in the mechanism involves the oxidation of acetaldehyde CH_3CHO, which takes place through various paths and produces a great diversity of products, including acetate ion CH_3COO^-, acetone CH_3COCH_3, crotonaldehyde $CH_3CH{=}CHCHO$, acetyl CH_3CO, methane, carbonate ion CO_3^{2-}, CO, CO_2, and other hydrocarbons. Most product species, as well as reactant species, will adsorb on the catalyst surfaces at lower potentials. The species of metal–OH, which is generated by dissociative adsorption of H_2O on the catalyst surface, enables the ethanol oxidation at low potentials,

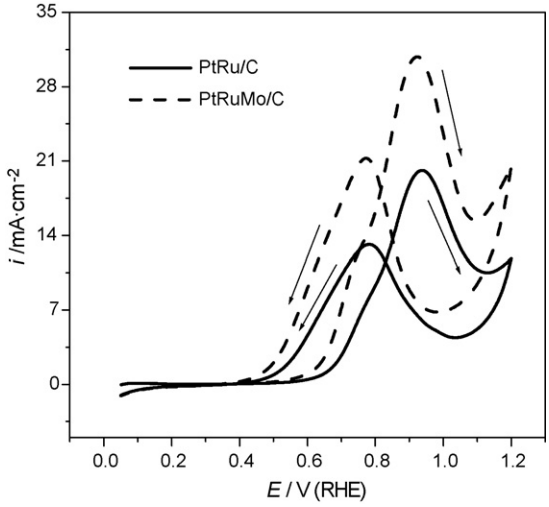

Fig. 4. Cyclic voltammograms of ethanol electrooxidation in an Ar-saturated solution of 0.5 mol L^{-1} CH_3CH_2OH and 0.5 mol L^{-1} H_2SO_4 at 25 °C on the PtRuMo/C and the Pt-Ru/C nanoparticles. Scan rate: 0.02 V s^{-1}.

but inhibits it at high potentials due to the strong association between –OH group and the catalyst surface. Therefore, when the cyclic-voltammetric measurement is performed with the thin film electrode in the solution of 0.5 mol L^{-1} CH_3CH_2OH and 0.5 mol L^{-1} H_2SO_4 at 25 °C with PtRuMo/C and PtRu/C as anodic catalysts, the current peaks, which is arising from the ethanol oxidation, can be observed in either the forward or the backward potential scanning process, as shown in Fig. 4. The performance of the PtRu/C nanoparticles presented here is the best available result obtained from various samples prepared by the same method and from the same precursors. Although the current-onset potentials near 0.55 V for both PtRuMo/C and PtRu/C are essentially the same, the peak current density of 30.8 mA cm^{-2} at the potential of 0.921 V (versus RHE) during the forward potential scanning process on PtRuMo/C can be distinguished clearly from that on PtRu/C, 20.1 mA cm^{-2} at 0.935 V. The backward scanning process results in the similar situation, 21.2 mA cm^{-2} at 0.774 V for PtRuMo/C compared with 13.2 mA cm^{-2} at 0.785 V for PtRu/C. In brief, the peak current of PtRuMo/C is about 10.7 mA cm^{-2} higher than that of PtRu/C, while its current-peak potential is about 14 mV lower than that of PtRu/C. Accordingly, the performance of PtRuMo/C for the ethanol electrooxidation can be considered superior to that of PtRu/C. The superposition of the two CV curves at low potentials (0.05–0.45 V) indicates the similarity of the two distinct catalysts in respects of the active sites and the specific area, which matches the result of the CO-stripping measurement.

For the anodic catalysts, the CO-tolerance can be evaluated with the steady-state current densities on the chronoamperometric curves, as depicted in Fig. 5, which was the result of measurement at 25 °C in the Ar-saturated solution system of 0.5 mol L^{-1} CH_3CH_2OH and 0.5 mol L^{-1} H_2SO_4 with the constant potential jump from 0.1 to 0.8 V. The initial high current corresponds mainly to double layer charging. Then the current decays with time in the parabolic style until reaching the apparent steady-state within 600 s. The high current density on the

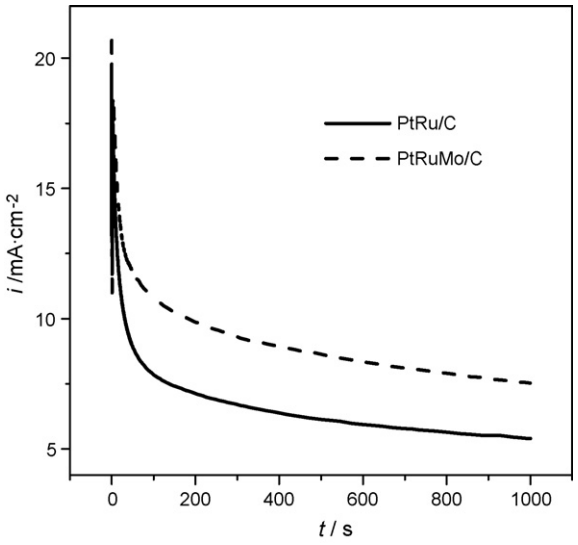

Fig. 5. Chronoamperometric curves of ethanol electrooxidation in an Ar-saturated solution of 0.5 mol L^{-1} CH_3CH_2OH and 0.5 mol L^{-1} H_2SO_4 at 25 °C on the PtRuMo/C and the PtRu/C nanoparticles. Potential jumps from 0.1 to 0.8 V.

PtRuMo/C nanoparticles, compared with that on the PtRu/C nanoparticles at the same potentials, indicates the superior CO-tolerance of PtRuMo/C, matching the above prediction of the cyclic voltammetry.

One of the requirements as catalysts for DEFC is the durability in the acidic solution, which can be roughly judged by the stabilized current densities on the amperometric *i–t* curves. The curves in Fig. 6 were obtained at 25 °C with PtRuMo/C and PtRu/C in the Ar-saturated solution of 0.5 mol L^{-1} CH_3CH_2OH and 0.5 mol L^{-1} H_2SO_4 at the fixed potential of 0.8 V (versus RHE). The current gradually decreases and finally stabilizes in about 60 min. The higher current density for PtRuMo/C, 3.6 mA cm^{-2} versus 2.1 mA cm^{-2} for PtRu/C at 10,000 s, further distinguishes the superiority of PtRuMo/C over PtRu/C, with respect to the catalytic activity and durability.

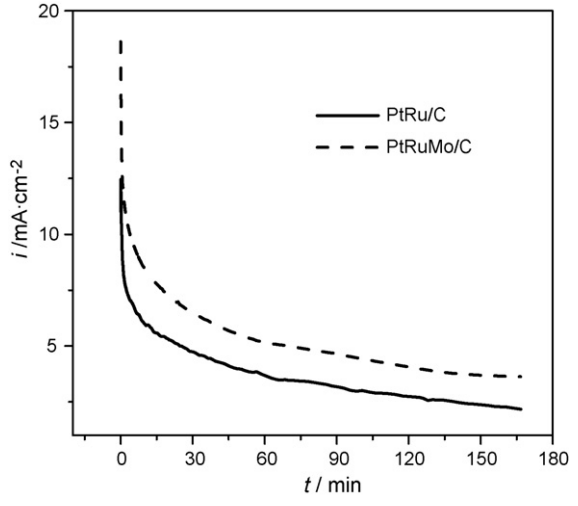

Fig. 6. Amperometric *i–t* curves of ethanol electrooxidation the PtRuMo/C and the PtRu/C nanoparticles in an Ar-saturated solution of 0.5 mol L^{-1} CH_3CH_2OH and 0.5 mol L^{-1} H_2SO_4 at 25 °C at a fixed potential of 0.8 V.

3.6. XPS revelation

Since many factors, including the particle morphology, particle size, particle structure, compositional homogeneity, and the electrochemically active specific area, have been excluded from causing the differentiation of the catalytic activity between the two nanoparticles catalysts, the PtRuMo/C and the PtRu/C, the attention is naturally drawn to their metal oxidation states on surfaces, for which the XPS analysis is appropriate in consideration of their suitable particle sizes.

The core level spectra of Pt 4f and Ru 3p for PtRuMo/C nanoparticles are depicted in Fig. 7a and b, respectively. The minor Ru 3p region was chosen to do analysis because the major Ru 5d region overlaps the carbon 1s region. The two most intense peaks in Fig. 7a, located at the binding energies of 70.95 eV (for Pt $4f_{7/2}$) and 74.33 eV (for Pt $4f_{5/2}$), maintain an area ratio near 4:3 as expected theoretically for pure Pt (71.20 eV of Pt $4f_{7/2}$ and 74.53 eV of Pt $4f_{5/2}$), and although their positions have been shifted lower [36]. Hence, there is no doubt that they originate from metallic Pt^0. The peaks at 71.72 and 75.82 eV can be attributed to Pt^{2+} in the form of PtO or $Pt(OH)_2$, which can be electrochemically reduced [36,38,50], while the peak at 74.56 eV arises from Pt^{4+}, possibly in PtO_2. The result of deconvolution indicates a phase composition which contains 72.7% of Pt in metallic Pt^0, 15.7% in Pt^{2+} (as PtO or $Pt(OH)_2$), and 10.6% in Pt^{4+} as PtO_2 [37,38,50]. In spite of the low intensity and therefore the relatively high background noise contribution in the Ru 3p core level region, the Ru $3p_{3/2}$ spectrum was deconvoluted into two peaks located at 459.92 and 462.52 eV, which are characteristic of Ru^0 and RuO_2, respectively [21,37,40]. The calculation shows that the large fraction of Ru (about 82.5%) is in the metallic state Ru^0, while a much smaller fraction exists as RuO_2 (about 17.5%).

The characteristic Mo doublet peak of $3d_{5/2}$ and $3d_{3/2}$ in Fig. 7c, which originates from the spin–orbit coupling effect, has to be treated cautiously, because a variety of Mo oxidation states contribute to this overlapping 3d region [50,51], among which Mo^{5+} is the most abundant species found in all samples and possibly existing as Mo_2O_5 or $MoO(OH)_3$ [52]. Through deconvolution of Mo 3d region of the spectra, the peaks can be associated with their corresponding oxidation states as follows: the Mo_2O_x peak (for $0 < x \leq 3$) is located in the region of 228.2–228.5 eV (where includes the previously reported Mo_2O_3 peak at 228.45 eV [50]), MoO_2 at 229.50 eV, Mo^{5+} at 231.05 eV, metallic Mo at 231.94 eV [26], and MoO_3 at around 232.60 eV, whereas the area ratio of $3d_{3/2}$ and $3d_{5/2}$ turns out to be 2:3.

Fig. 8a and b illustrates the data for PtRu/C in the similar way. The spectrum of Pt 4f (70.98 eV of Pt $4f_{7/2}$ and 74.40 eV of Pt $4f_{5/2}$) for PtRu/C in Fig. 8a resembles that in Fig. 7a for PtRuMo/C. It manifests that in the PtRu/C system Pt contains 70.7% of metallic Pt^0, 16.8% of Pt^{2+} (as PtO or $Pt(OH)_2$), and 13.5% of Pt^{4+} (as PtO_2). Similarly, the Ru 3p spectrum in Fig. 8b demonstrates that Ru is composed of 85.7% of metallic Ru and 14.3% of RuO_2.

Considering the notable observation that no peak arising from other elements appears in the systems of both PtRuMo/C

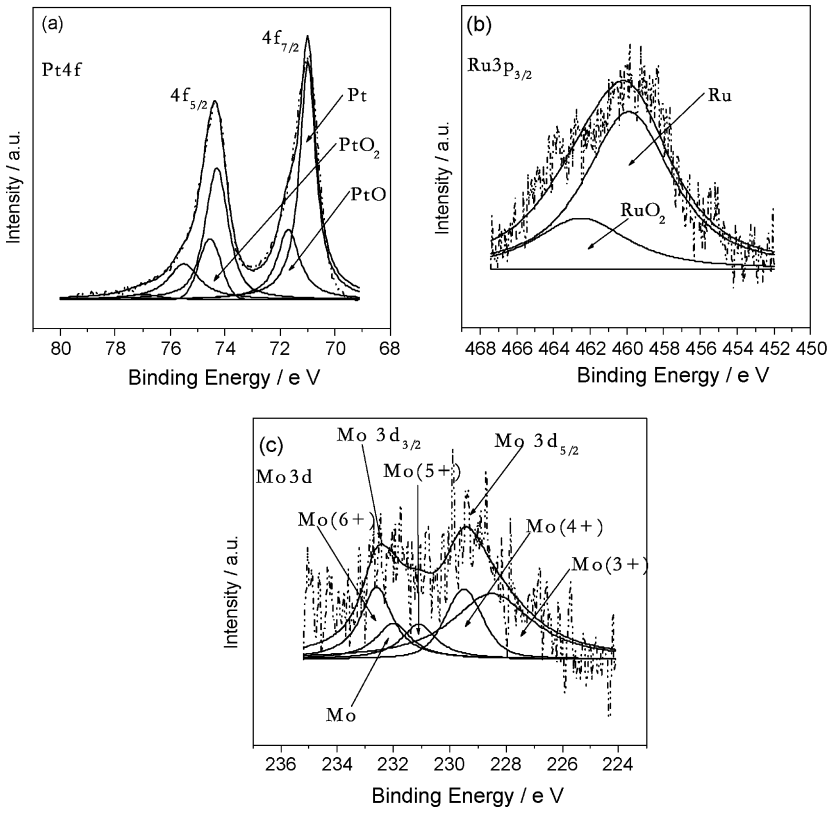

Fig. 7. XPS core level spectra for the (a) Pt 4f, (b) Ru 3p, and (c) Mo 3d photoemission from the PtRuMo/C nanoparticles.

and PtRu/C, there is no doubt here that the ions from other metal salts were completely removed during their pretreatment process.

3.7. Analysis of Mo influence

The enhanced performance of PtRuMo/C nanoparticles electrocatalyst, compared with that of PtRu/C, has hereby been ascribed to Mo additive, the effect of which can be explored from three aspects: the bifunctional mechanism, the hydrogen-spillover phenomena, and the modification of Pt electronic states.

The bifunctional mechanism has been established in the previous studies as follows [28]:

$$MoO_x + H_2O \rightarrow (MoO_x)\text{-}OH_{ads} + H^+ + e^- \quad (7)$$

$$Pt\text{-}(CO)_{ads} + (MoO_x)\text{-}OH_{ads} \rightarrow CO_2 + H^+ + Pt + MoO_x + e^- \quad (8)$$

It can be seen that MoO_x promotes the water activation, which generates the species of $-OH_{ads}$ to oxidize CO subsequently. This accounts for the enhanced activity of the PtRuMo/C nanoparticle catalyst during the process of ethanol electrooxidation.

On the other hand, recent researches on Pt-WO_x nanophases indicated that hydrogen on the top site of Pt atom could migrate to the site over WO_x at the positive potential in such a process that can be described with the following Eq. (9) [23,53,54]:

$$Pt\text{-}H + WO_x \rightarrow Pt + H\text{-}WO_x \quad (9)$$

which is the so-called "hydrogen spillover" from Pt to WO_x. The transfer of hydrogen liberates the Pt active sites, which otherwise would have been blocked by hydrogen during the electrooxidation of methanol. A similar situation in PtRuMo/C nanoparticles can be imagined here, with the following proposed scheme of the hydrogen-spillover process [29]:

$$MoO_x + Pt\text{-}H_{ads} \rightarrow HMoO_x + Pt \quad (10)$$

Such a process relieves the CO-style poisoning process caused by the adsorption of hydrogen.

In addition, as the Mo oxides consist of mixed-valences, MoO_x are relatively stable in acid solution and have relatively high electronic conductivities in the surface of the PtRuMo/C nanoparticles, owing to their rutile-type structure with the short metal–metal distance along the shared edges [28,29].

Finally, the data in Figs. 7 and 8 indicate clearly that the shift of the Pt spectra increases by adding the Mo into the catalyst systems, although there is no obvious quantitative relationship. The increased shift with Mo can be considered as the evidence that Mo modifies the electronic states of Pt. The modification of electronic states for Pt may subsequently change the catalytic activity of platinum in the ethanol electrooxidation process. In addition, the transfer of the electron density from Mo to Pt may occur, since the electronegativity of Mo is 1.96 while that of Pt is 2.28. The apparent effect is that the catalytically active sites

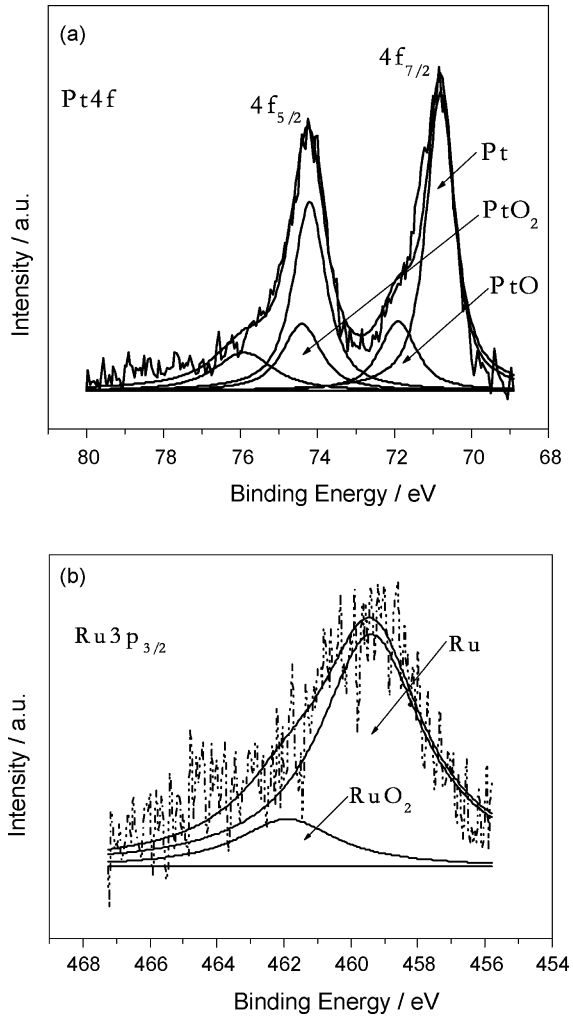

Fig. 8. XPS core level spectra for the (a) Pt 4f and (b) Ru 3p photoemission from the PtRu/C nanoparticles.

are increased because the coverage of CO_{ads} on the Pt surface is reduced due to the decreased Pt-CO binding energy.

In summary, the improved performance of PtRuMo/C nanoparticles may be the cooperative result of the bifunctional mechanism, the hydrogen-spillover effect, and the modification of the Pt electronic states. And the further investigations will clarify the intrinsic mechanism of this catalyst.

4. Conclusions

For the ethanol electrooxidation in H_2SO_4 solution, the PtRuMo/C nanoparticle catalyst, formed through the reduction of inorganic precursor salts with $NaBH_4$, is superior to the similarly synthesized PtRu/C catalyst, in aspects of the catalytic activity, the CO-tolerance, and the durability in the acidic solutions. Most common factors, including the particle size, morphology, the compositional homogeneity, and the electrochemically active specific area, have been excluded from playing the major roles to distinguish PtRuMo/C as the superior catalyst when it is compared with PtRu/C. The effect of Mo in the PtRuMo/C nanoparticles is explained through the bifunctional mechanism, the hydrogen-spillover effect, and the modification of the Pt electronic states.

The enhanced activity of the PtRuMo/C nanoparticle is surely throwing some light on the research and development of effective DEFC catalysts. The experiments to further illustrate the rule of Mo are on the way, with the catalysts dispersed in the membrane electrode assembly (MEA) to be evaluated in the DEFC single-cell test. The future project includes the life-testing process to observe the long-term performance of catalysts.

Acknowledgements

This research is financially supported by the National Natural Science Foundation of China (Grant No. 20606007), Heilongjiang Natural Science Foundation (B0201), and Harbin Institute of Technology (HIT 2002.39).

References

[1] H. Uchida, Y. Mizuno, M. Watanabe, J. Electrochem. Soc. 149 (2002) A682–A687.
[2] W.C. Choi, J.D. Kim, S.I. Woo, Catal. Today 74 (2002) 235–240.
[3] Z.B. Wang, G.P. Yin, P.F. Shi, Carbon 44 (2006) 133–140.
[4] C. Lamy, E.M. Belgsir, J.-M. Leger, J. Appl. Electrochem. 31 (2001) 799–809.
[5] E.V. Spinace, A.O. Neto, M. Linardi, J. Power Sources 124 (2003) 426–431.
[6] W.J. Zhou, S.Q. Song, W.Z. Li, Z.H. Zhou, G.Q. Sun, Q. Xin, S. Douvartzides, P. Tsiakaras, J. Power Sources 140 (2005) 50–58.
[7] Z.B. Wang, G.P. Yin, J. Zhang, Y.C. Sun, P.F. Shi, J. Power Sources 160 (2006) 37–43.
[8] G.A. Camara, R.B. de Lima, T. Iwasita, Electrochem. Commun. 6 (2004) 812–815.
[9] C. Lamy, S. Rousseau, E.M. Belgsir, C. Coutanceau, J.-M. Leger, Electrochim. Acta 49 (2004) 3901–3908.
[10] N. Fujiwara, K.A. Friedrich, U. Stimming, J. Electroanal. Chem. 472 (1999) 120–125.
[11] F. Vigier, C. Coutanceau, A. Perrard, E.M. Belgsir, C. Lamy, J. Appl. Electrochem. 34 (2004) 439–446.
[12] E.V. Spinace, A.O. Neto, T.R.R. Vasconcelos, M. Linardi, J. Power Sources 137 (2004) 17–23.
[13] E.V. Spinace, A.O. Neto, M. Linardi, J. Power Sources 129 (2004) 121–126.
[14] A.O. Neto, M.J. Giz, J. Perez, E.A. Ticianelli, E.R. Gonzalez, J. Electrochem. Soc. 149 (2002) A272–A279.
[15] S. Ball, A. Hodgkinson, G. Hoogers, S. Maniguet, D. Thompsett, B. Wong, Electrochem. Solid-State Lett. 5 (2002) A31–A34.
[16] F. Vigier, C. Coutanceau, F. Hahn, E.M. Belgsir, C. Lamy, J. Electroanal. Chem. 563 (2004) 81–89.
[17] S. Pick, Surf. Sci. 436 (1999) 220–226.
[18] V.P. Santos, G. Tremiliosi-Filho, J. Electroanal. Chem. 554–555 (2003) 395–405.
[19] W.J. Zhou, W.Z. Li, S.Q. Song, Z.H. Zhou, L.H. Jiang, G.Q. Sun, Q. Xin, K. Poulianitis, S. Kontou, P. Tsiakaras, J. Power Sources 131 (2004) 217–223.
[20] B. Gurau, R. Viswanathan, R.X. Liu, T.J. Lafrenz, K.L. Ley, E.S. Smotkin, E. Reddington, A. Sapienza, B.C. Chan, T.E. Mallouk, S. Sarangapani, J. Phys. Chem. B 102 (1998) 9997–10003.
[21] F.J. Rodriguez-Nieto, T. Morante-Catacora, C.R. Cabrera, J. Electroanal. Chem. 571 (2004) 15–26.
[22] M. Umeda, H. Ojima, M. Mohamedi, I. Uchida, J. Power Sources 136 (2004) 10–15.
[23] M. Gotz, H. Wendt, Electrochim. Acta 43 (1998) 3637–3644.
[24] Z.B. Wang, G.P. Yin, J. Zhang, Y.C. Sun, P.F. Shi, Electrochim. Acta 51 (2006) 5691–5697.
[25] G. Samjeske, H. Wang, T. Loffler, H. Baltruschat, Electrochim. Acta 47 (2002) 3681–3692.

[26] B.N. Grgur, N.M. Markovic, P.N. Ross, J. Phys. Chem. B 102 (1998) 2494–2501.
[27] B.N. Grgur, N.M. Markovic, P.N. Ross, J. Electrochem. Soc. 146 (1999) 1613–1619.
[28] Y. Wang, E.R. Fachini, G. Cruz, Y.M. Zhu, Y. Ishikawa, J.A. Colucci, C.R. Cabrera, J. Electrochem. Soc. 148 (2001) C222–C226.
[29] H.Q. Zhang, Y. Wang, E.R. Fachini, C.R. Cabrera, Electrochem. Solid-State Lett. 2 (1999) 437–439.
[30] S. Mukerjee, S.J. Lee, E.A. Ticianelli, J.B. McBreen, N. Grgur, N.M. Markovic, P.N. Ross, J.R. Giallombardo, E.S. de Castro, Electrochem. Solid-State Lett. 2 (1999) 12–15.
[31] E.I. Santiago, G.A. Camara, E.A. Ticianelli, Electrochim. Acta 48 (2003) 3527–3534.
[32] E.G. Neto, E. Franco, M. Arico, E.R. Linardi, Gonzalez, J. Eur. Ceram. Soc. 23 (2003) 2987–2992.
[33] Z.B. Wang, G.P. Yin, P.F. Shi, Y.C. Sun, Electrochem. Solid-State Lett. 9 (2006) A13–A15.
[34] T.J. Schmidt, H.A. Gasteiger, G.D. Stab, P.M. Urban, D.M. Kolb, R.J. Behm, J. Electrochem. Soc. 145 (1998) 2354–2358.
[35] K.W. Park, J.H. Choi, B.K. Kwon, S.A. Lee, Y.E. Sung, H.Y. Ha, S.A. Hong, H.S. Kim, A. Wieckowski, J. Phys. Chem. B 106 (2002) 1869–1877.
[36] C. Bock, C. Paquet, M. Couillard, G.A. Botton, B.R. MacDougall, J. Am. Chem. Soc. 126 (2004) 8028–8037.
[37] A.K. Shukla, A.S. Arico, K.M. El-Khatib, H. Kim, P.L. Antonucci, V. Antonucci, Appl. Surf. Sci. 137 (1999) 20–29.
[38] Y.M. Liang, H.M. Zhang, Z.Q. Tian, X.B. Zhu, X.L. Wang, B.L. Yi, J. Phys. Chem. B 110 (2006) 7828–7834.
[39] T.C. Deivaraj, W.X. Chen, J.Y. Lee, J. Mater. Chem. 13 (2003) 2555–2560.
[40] C.Z. He, H.R. Kunz, J.M. Fenton, J. Electrochem. Soc. 144 (1997) 970–979.
[41] L. Giorgi, A. Pozio, C. Bracchini, R. Giorgi, S. Turtu, J. Appl. Electrochem. 31 (2001) 325–334.
[42] Z.B. Wang, G.P. Yin, P.F. Shi, J. Electrochem. Soc. 152 (2005) A2406–A2412.
[43] P.J. Ferreira, G.J. Lao, Y. Shao-Horn, D. Morgan, R. Makharia, S. Kocha, H.A. Gasteiger, J. Electrochem. Soc. 152 (2005) A2256–A2271.
[44] A. Pozio, M. de Francesco, A. Cemmi, F. Cardellini, L. Giorgi, J. Power Sources 105 (2002) 13–19.
[45] C.L. Green, A. Kucernak, J. Phys. Chem. B 106 (2002) 1036–1047.
[46] C. Lamy, A. Lima, V. LeRhun, F. Delime, C. Coutanceau, J.-M. Leger, J. Power Sources 105 (2002) 283–296.
[47] Z.S. Jin, C.J. Xi, Q.M. Zeng, F. Yin, J.Z. Zhao, J.Z. Xue, J. Mol. Catal. A Chem. 191 (2003) 61–66.
[48] S.L. Douvartzides, P.E. Tsiakaras, J. Catal. 211 (2002) 521–529.
[49] S.A. Kirillov, P.E. Tsiakaras, I.V. Romanova, J. Mol. Struct. 651–653 (2003) 365–370.
[50] S. Zafeiratos, G. Papakonstantinou, M.M. Jacksic, S.G. Neophytides, J. Catal. 232 (2005) 127–136.
[51] D.L. Sullivan, J.G. Ekerdt, J. Catal. 172 (1997) 64–75.
[52] S. Mukerjee, R.C. Urian, Electrochim. Acta 47 (2002) 3219–3231.
[53] K.-W. Park, J.-H. Choi, K.-S. Ahn, Y.-E. Sung, J. Phys. Chem. B 108 (2004) 5989–5994.
[54] K.-W. Park, K.-S. Ahn, Y.-C. Nah, J.-H. Choi, Y.-E. Sung, J. Phys. Chem. B 107 (2003) 4352–4355.